Bifurcation study of a semiconductor laser with saturable absorber and delayed optical feedback

Bernd Krauskopf and Jamie Walker, University of Bristol, UK

February 2011

1 Introduction

Semiconductor lasers are a very efficient type of laser that has found numerous applications in recent years — most prominently in optical data storage and in optical telecommunication. Indeed, fiber-optic communication has become the method of choice for transmitting large amounts of information, and semiconductor laser devices are the optical light sources behind today's telecommunication networks. There are many reasons for the popularity of this type of laser as a light source: semiconductor lasers are very efficient in converting electrical energy into coherent light, very small (with cavity lengths of about 1 mm), and cheap and easy to manufacture. From a more fundamental perspective, a semiconductor laser is a damped nonlinear oscillator. It is now well known that, apart from stable emission, semiconductor laser systems may show a wealth of other dynamics, including different types of periodic output, as well as quasiperiodic and chaotic dynamics. This type of dynamics are brought about by external influences, such as modulation of the electrical pump current, external optical input or optical feedback. See, for example, Refs. [1, 2] as entry points to the extensive literature on nonlinear laser dynamics.

The focus of this study is a semiconductor laser with saturable absorber (SLSA), which has been shown experimentally [3] and theoretically [4, 5] to be capable of producing self-pulsations. The underlying physical process is called passive Q-switching, and it can be explained as follows; see also [6, 7]. The absorber in (or adjacent to) the laser cavity acts as a store of energy that is supplied to the semiconductor laser by an electrical pump current. Filling this energy store is a relatively slow process (with respect to the internal time scale of the laser dynamics). When the absorber is saturated then the laser is able to overcome its losses and all the stored energy is released in a very short period of time, leading to a pulse of emitted light. The intensity drops back to zero and the process repeats. The result is a pulse train with a typical pulse-repetition frequency on the order of several GHz.

It is this property of the SLSA that makes it interesting for use in pulse generation for telecommunication and for optical clocks. However, there is one drawback: the self-sustained oscillations may be quite sensitive to the influence of external or internal noise [8]. More specifically, when the absorber is close to being saturated the next pulse can be triggered by even quite small amounts of noise. The result of noise is so-called timing jitter of the pulses, meaning that the time in between successive pulses is subject to considerable fluctuations.

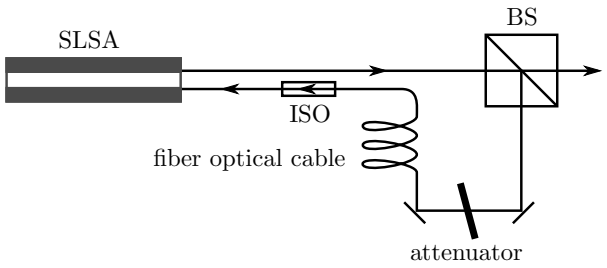

Figure 1: Sketch of an SLSA (illustrated by a (white) gain medium surrounded by a (grey) absorber medium) that is fed back a part of its output via an external optical feedback loop with fixed delay time, as determined by a length of fiber optical cable; the feedback loop also includes a beam splitter (BS), an optical isolator (ISO) and an attenuator.

The system actually displays what is known as coherence resonance: there is a noise level that minimises the timing jitter of the pulse train of the SLSA; see Ref. [9]. Clearly any considerable jitter due to noise is detrimental in the mentioned applications, because they require precise timing of pulses.

It has been shown that the timing jitter of the SLSA is due to the fact that self-sustained pulsations occur close to a region of excitability [5, 9]. Excitability is a well-known concept that comes originally from biology and chemistry [10]. Examples are excitation waves in reaction-diffusion systems, such as cardiac muscle tissue and the Belousov-Zhabotinsky reaction [11]; excitability is also an important concept in neuron and cell modelling, and it is one of the mechnisms that may lead to the spiking of nerve cells [10, 12]. More recently there has been a surge of interest in excitable laser systems. Indeed, lasers with saturable absorber are not the only class of lasers in which excitability has been found. Other laser systems demonstrating excitability include lasers with optical injection [13, 14] or optical feedback [15, 16], multisection DFB lasers [17], and lasers with integrated dispersive reflectors [18]; see also Ref. [19]. Potential applications of excitable lasers include clock recovery, where the laser acts as an optical switch that reacts only to sufficiently large optical input, and pulse reshaping, where a dispersed input pulse can generate a clean large-amplitude output pulse.

In this chapter we consider the dynamics of the SLSA when part of its output light is fed back after a given delay time τ. This laser system can be realized as is sketched in Figure 1. A beam splitter (BS) diverts a part of the laser's output into a feedback loop. The feedback strength κ can be varied by an attenuator, and the delay time τ is determined by a chosen length of fiber optical cable; an optical isolator (ISO) prevents unwanted back-reflections. One motivation for studying this setup is to understand how to operate the SLSA with delayed optical feedback in such a way that it produces a pulse train with desired properties. The naive underlying idea is the following. Suppose that the SLSA is in the excitable regime (in the absence of feedback). When a first

pulse is triggered then a part of it will travel back to the SLSA via the feedback loop to trigger the next pulse. If this process continues stably, then a train of pulses will be generated. Importantly, the frequency of the pulse train is determined by the delay time τ of the external feedback loop (and not just by the material properties of the SLSA). Hence, the SLSA with delayed optical feedback features two additional control parameters, the delay time τ and the feedback strength κ. The main question is how these two external parameters influence the dynamics of the overall system, given the properties of the SLSA as determined by its internal parameters.

To answer this question we perform a bifurcation study of the SLSA with delayed optical feedback as modeled by the established Yamada rate equations [20] for the gain G, the absorption Q and the intensity I, to which a delay term has been added. When written in dimensionless form one obtains the system

$$\dot{G} = \gamma\left(A - G - GI\right), \tag{1}$$

$$\dot{Q} = \gamma\left(B - Q - aQI\right), \tag{2}$$

$$\dot{I} = \left(G - Q - 1\right) I + \kappa I\left(t - \tau\right), \tag{3}$$

where the dot denotes derivation with respect to time. The delay term $\kappa I\left(t-\tau\right)$, with feedback strength $\kappa \geq 0$ and delay time $\tau \geq 0$, models the feedback via the external optical loop. Physically, the length l of the feedback loop, which is mainly due to the fiber optical cable, determines the single fixed delay $\tau = l/c > 0$ where c is the speed of light.

For $\kappa = 0$ one recovers the Yamada equations — a system of three first-order ordinary differential equations (ODEs) that describe a single-mode laser with saturable absorber — in the form that was considered for the bifurcation study in Ref. [5]. There are four dimensionless parameters: the pump parameter A of the gain, the pump parameter B of the absorption, the cross-saturation coefficient a, and the time-scale ratio γ between the relaxation rates (or decay times) of gain and absorber. For physical reasons the parameter space of Eqs. (1)–(3) for $\kappa = 0$ is confined to $A \geq 0$, $B \geq 0$, $a \geq 1$, and $\gamma \geq 0$. Furthermore, γ is a small parameter (of the order of $10^{-3} - 10^{-4}$), which means that gain G and absorption Q evolve on a much slower time scale than the intensity I. Hence, the SLSA is an example of a slow-fast system with an explicit splitting of time scales; see, for example, Ref. [21]. A complete bifurcation analysis of Eqs. (1)–(3) for $\kappa = 0$ can be found in Ref. [5]. In particular, just before the onset of naturally occurring self-pulsations the dynamics of the SLSA is excitable [5, 9]; these results are summarized in Section 2, and they form the basis of what is presented here.

To address the question of how the dynamics of the SLSA is influenced by the external feedback loop, we present a bifurcation study of Eqs. (1)–(3) for $\kappa \geq 0$. Note that this means that we are dealing with a system of delay differential equations (DDEs) with a single fixed delay. As such it has as its phase space the space $C[-\tau, 0]$ of continuous functions over the delay interval $[-\tau, 0]$ with values in (G, Q, I)-space; see, for example, Refs. [22, 23, 24]. It is this element of infinite-dimensionality that allows Eqs. (1)–(3) to show much richer dynamics

than the SLSA alone (when $\kappa = 0$). Up until only a few years ago, practical methods for analyzing DDEs were limited to linearization around equilibria of the system and numerical integration of the governing equations. Today, however, numerical tools for the detection and continuation in parameters of equilibria, periodic solutions and their bifurcations are also available for DDEs in the form of the packages DDE-BIFTOOL [25] and PDDE-CONT [26]; see also the recent surveys Refs. [27, 28]. We use here the package DDE-BIFTOOL to carry out a bifurcation study of the full DDE given by Eqs. (1)–(3). More specifically, we fix $B = 5.8$, $a = 1.8$, $\gamma = 0.04$ throughout and consider bifurcation diagrams in the (τ, κ)-plane, where we consider two main cases for the gain pump rate A: one where the SLSA is off and excitable, and the other where it is is off and not excitable. The transition between these two cases as A is changed is explained in terms of the passage through codimension-three bifurcation points.

In light of the explicit split into slow and fast variables of the system, what is presented here is a case study of a slow-fast system subject to delayed feedback. This more general aspect provides a second motivation, because it may also be of interest for other areas of application. For example, the issue of delayed feedback or coupling also arizes in the context of interacting (populations of) neuron cells, which themselves may display dynamics on separate time scales.

The chapter is organized as follows. In Section 2 we summarize the results from Ref. [5] for $\kappa = 0$. The next four sections are devoted to the study of the full DDE for $\kappa \geq 0$. Section 3 presents analytic results on basic bifurcations of equilibria. Sections 4 and 5 are devoted to bifurcation diagrams in the (τ, κ)-plane for two representative values of the gain pump parameter A, and Section 6 discusses the transition between them via different codimension-three bifurcations. Finally, we summarize in Section 7.

2 Bifurcation analysis of the SLSA

The Yamada model in the form of Eqs. (1)–(3) for $\kappa = 0$ describes a semiconductor laser with saturable absorber in two different geometric configurations: (i) in a sectional configuration where there are gain and absorber sections inside the laser cavity but with the same carrier life-time, and (ii) in a stripe confguration where unpumped side regions act as the absorber (as in Figure 1).

Figure 2 summarizes the main results of a bifurcation analysis of the Yamada model in Ref. [5]. The main object is the two-parameter bifurcation diagram in the (A, γ)-plane of pump paramter A of the gain and time-scale separation parameter γ, where the pump parameter B of the absorption and the cross-saturation coefficicent a have fixed values. We are concerned with the bifurcation diagram of type III (in the notation of Ref. [5]), because it features all possible dynamics of the SLSA. This bifurcation diagram is sketched diagramatically in Figure 2(a), and it is shown in panel (b) as computed with the continuation package AUTO [31] for $(B, a) = (5.8, 1.8)$. The bifurcation diagram of type III is physically relevant because it can be found for any sufficiently

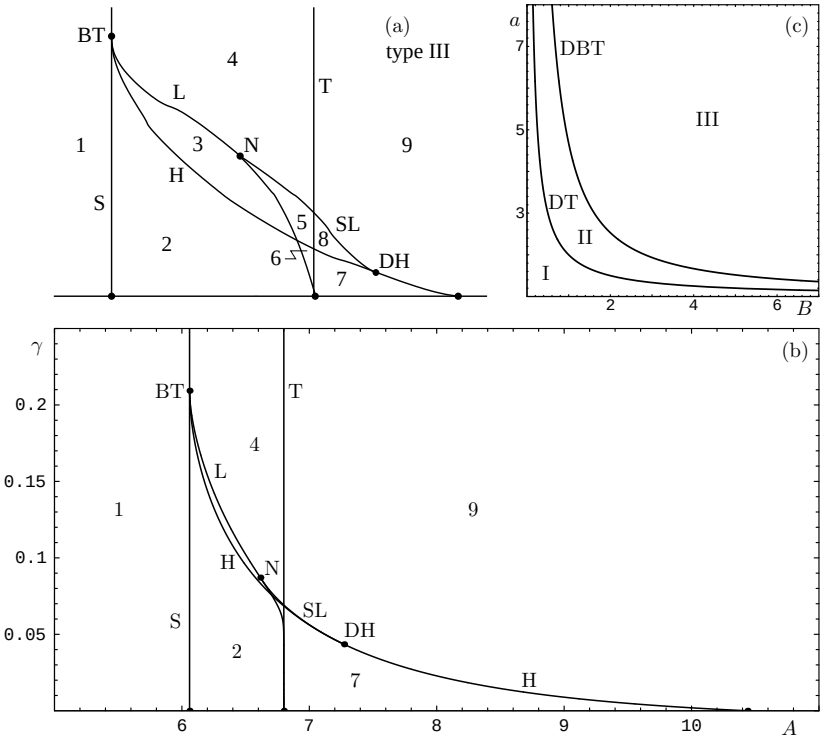

Figure 2: Bifurcation diagram from Ref. [5] of the Yamada model, Eqs. (1)–(3) for $\kappa = 0$. Panel (a) is a sketch of the bifurcation diagram of type III in the (A, γ)-plane of gain pump parameter A and time-scale separation parameter γ; panel (b) shows this bifurcation diagram in the (A, γ)-plane as computed for $(B, a) = (5.8, 1.8)$; see Figure 3 for the corresponding phase portraits in regions 1–9. Panel (c) shows the division of the (B, a)-plane of absorption pump parameter B and cross-saturation coefficicent a into regions of bifurcation diagrams of types I–III.

large values of B and a. This is illustrated in Figure 2(c), which shows how the (B, a)-plane is divided (by two curves DT and DBT of two different types of degenerate Bogdanov-Takens bifurcations) into three regions corresponding to bifurcation diagrams of types I–III. The bifurcation diagrams of types I and II (which are not considered here) can be found in Ref. [5].

We now discuss the bifurcation diagram of type III in Figure 2(a) and (b) in more detail; see, for example, Refs. [29, 30] as general references to bifurcation theory. Several bifurcation curves divide the (A, γ)-plane into nine regions of topologically different phase portraits, which can be found in panels 1–9 of Figure 3. The phase portraits are represented as two-dimensional sketches because, after possible transients, the dynamics takes place in a globally attracting two-

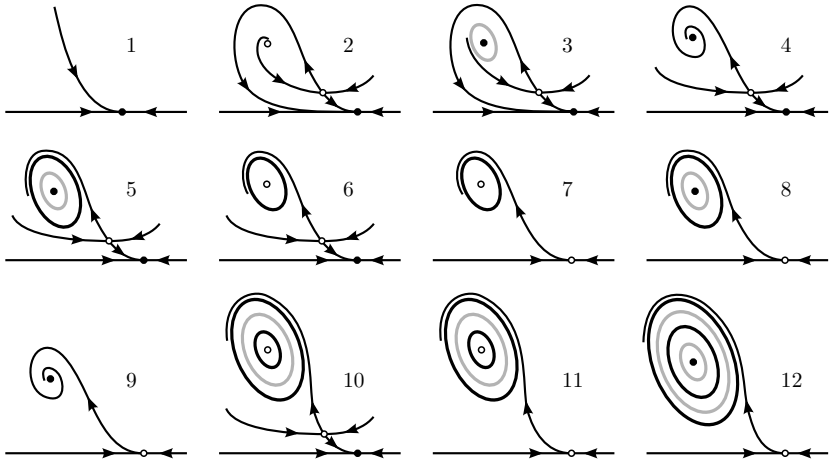

Figure 3: Phase portraits corresponding to the numbered regions 1–9 in Figure 2 and regions 1–12 in Figures 6 and 9. Shown are two-dimensional sketches in projection onto the (G, I)-plane, where the invariant set $\{I = 0\}$ is at the bottom; the third direction that is not shown is attracting. Black dots are attracting equilibria; open dots are saddle equilibria, and they have stable and unstable manifolds; black closed curves are attracting periodic orbits, and grey closed curves are saddle periodic orbits.

dimensional surface that is close to $\{G - Q - 1 = 0\}$; the third direction that is not shown in Figure 3 is consequently attracting. Along each bifurcation curve in the (A, γ)-plane one finds a particular bifurcation (qualitative change of the dynamics), which is said to be of codimension one; specifically, we encounter:

- a saddle-node bifurcation curve S, where two equilibria are created (or disappear); an example is the transition between phase portraits 1 and 2;
- a transcritical bifurcation curve T, where an equilibrium for $I = 0$ changes stability by an equilibrium moving out of (or into) the region for $I > 0$; an example is the transition between phase portraits 4 and 9;
- a Hopf bifurcation curve H, where a periodic orbit (corresponding to self-oscillations) is created (or disappears); an example is the transition between phase portraits 2 and 3;
- a curve L along which one finds a homoclinic loop to a saddle equilibrium; a periodic orbit bifurcates from this homoclinic loop; an example is the transition between phase portraits 3 and 4;
- a curve SL of saddle-node bifurcation of limit cycles, where two periodic orbits (one attracting and one of saddle type) are created (or disappear); an example is the transition between phase portraits 4 and 5.

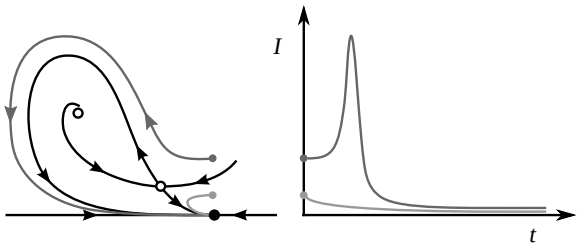

Figure 4: The excitable phase portrait 2 (left) gives rise to a pulse for a sufficiently large perturbation from the off-state (right).

The bifurcation diagram in Figure 2(a) and (b) is organized by a number of special points — known as codimension-two bifurcations — where several bifurcation curves come together. The main organizing center is a Bogdanov-Takens point BT on the curve S (characterized by a double zero eigenvalue of the Jacobian at the equilibrium), from which the curves H and L emerge. The homoclinic loop curve L changes type in a codimension-two point N (where the saddle quantity of the equilibrium in the homoclinic loop becomes zero and changes sign); here the bifurcating periodic orbit changes from repelling (in region 3) to attracting (in region 5). From N the curve SL emerges and it ends on the Hopf curve H at a point DH of degenerate Hopf bifurcation; note from Figure 2(b) that the curve SL is very close to the Hopf curve H. The homoclinic loop curve L ends at the bottom point of the transcritical curve T (where $\gamma = 0$); notice that the curve L follows the curve T extremely closely for $\gamma < 0.05$; see Figure 2(b).

One conclusion from Figures 2 and 3 is that, for realistically small values of the time-scale separation parameter γ, one finds a unique sequence of bifurcations as the gain pump parameter A is increased. Note in this context that A is the only parameter that can be changed during an experiment. Initially, the laser is off, which is represented in region 1 by an attractor with intensity $I = 0$. When the curve S is crossed, the laser is still off in region 2, but there are now two additional equilibria; both are saddle points in (G, Q, I)-space with $I > 0$. (Recall that the missing direction in Figures 3 is attracting.) When A is increased further, the homoclinic loop curve L and the transcritical curve T are practically crossed at the same time; this marks the onset of self-pulsations, which are represented in region 7 by an attracting periodic orbit. We remark that region 6, where one finds coexistence of the stable equilibrium and a stable periodic orbit, is so small that it was not found in studies that changed A for fixed small γ. Yet, region 6 must exist for topological reasons, and it was indeed found only as part of the bifurcation diagram of type III by allowing γ to take larger values. Finally, when A is increased even further, the Hopf bifurcation curve H is crossed. The self-pulsations disappear and the laser produces light with constant intensity I; in region 9 this is represented by a globally attracting equilibrium.

It is an important realization that the SLSA is excitable in region 2, that is, for a considerable range of the gain pump parameter A. Figure 4 shows the underlying mechanism in more detail. The laser is in its off-state and this is represented by the globally attracting equilibrium with $I = 0$. In response to any sufficiently small perturbation in the intensity I, the SLSA relaxes back to the off-state. On the other hand, any perturbation above a certain threshold results in a large pulse before the SLSA relaxes back to the off-state; one speaks of the excitability threshold, and it is given in this case by the stable manifold of the saddle point that lies close to the stable equilibrium. Physically, the perturbation in I is sufficient in this case to overcome the losses and release the energy stored in the absorber. The SLSA requires what is known as a refractory period (to recharge the absorber) before the next pulse can be triggered. Note that the saddle point moves closer to the attractor as the transcritical curve T is approached, which implies that the excitablility threshold decreases. Hence, in region 2 the SLSA becomes more and more likely to produce noise-induced pulses as A is increased.

3 Equilibria of the DDE and their stability

If we now consider $k \geq 0$ then Eqs. (1)–(3) are a system of DDEs and, as such, difficult to study by analytical means. Nevertheless, it is possible to find explicit formulas for some of their bifurcations. This information provides the basis of the numerical bifurcation analysis in the next sections.

There are three equilibra, E_1, E_2 and E_3, given by

$$E_1 : (G, Q, I) = (A, B, 0), \tag{4}$$

$$E_2, E_3 : (G, Q, I) = \left(\frac{A}{1 + I_\pm}, \frac{B}{1 + aI_\pm}, I_\pm \right), \tag{5}$$

where

$$I_\pm = \frac{-aA + b + a + 1 - a\kappa - \kappa}{2a(\kappa - 1)} \pm \frac{\sqrt{(aA - B - a - 1 + a\kappa + \kappa)^2 - 4a(\kappa - 1)(A - B - 1 + \kappa)}}{2a(\kappa - 1)}. \tag{6}$$

The equilibrium E_1 lies on the invariant plane $\{I = 0\}$; it exists for all values of the parameters and corresponds to the non-lasing solution. The two equilibria E_2 and E_3 have non-zero intensity and, since $2a(\kappa - 1) \leq 0$ for all $\kappa \in [0, 1]$, we find that $I_- > I_+$. That is, the intensity value at E_2 is less than that at E_3. Note that for $\kappa = 0$ the intensity equation for $I_\pm$ reduces to that for the Yamada model [5].

To check the stability and bifurcations of the equilibria we make use of the fact that Eqs. (1)–(3) are a DDE with a single fixed delay $\tau > 0$, which has the general form

$$\dot{\mathbf{x}} = f(\mathbf{x}(t), \mathbf{x}(t - \tau), \psi) =: f(u, v, \psi).$$

Here $\mathbf{x}(t) \in \mathbb{R}^3$ represents a point in the physical (G, Q, I)-space and f is a smooth function that depends on the parameter vector ψ. The stability of an equilibrium $\mathbf{x}_0$ is determined by the roots λ of the characteristic equation

$$\det\left(\lambda(\delta_{ij}) - A_1 - A_2 e^{-\lambda\tau}\right) = 0$$

where

$$A_1 = \frac{\partial f(\mathbf{x}_0)}{\partial u}, \quad A_2 = \frac{\partial f(\mathbf{x}_0)}{\partial v}$$

and (δ_{ij}) is the identity matrix. The transcendental characteristic equation evaluated at an equilibrium has countably infinitely many roots λ_i, but only finitely many of them have a positive real part. Hence, an equilibrium is either an attractor with infinitely many attracting directions, or a saddle point with a finite number of repelling directions and an infinite number of attracting directions; see Refs. [22, 23, 24].

For Eqs. (1)–(3) we have

$$A_1 = \begin{bmatrix} -\gamma(1+I) & 0 & -\gamma G \\ 0 & -\gamma(1+aI) & -\gamma aQ \\ I & -I & G-Q-1 \end{bmatrix}, \qquad A_2 = \begin{bmatrix} 0 & 0 & 0 \\ 0 & 0 & 0 \\ 0 & 0 & \kappa \end{bmatrix},$$

and the characteristic equation is

$$\begin{aligned} 0 \;=\; & \lambda^3 + [1 - G + Q + \gamma(2 + aI + I) - \kappa e^{-\lambda\tau}]\lambda^2 \\ & + [\gamma^2(1 + I + aI + aI^2) + \gamma(2 - 2G + 2Q + I \\ & \qquad + aI - aGI + QI) - \gamma(2 + I + aI)\kappa e^{-\lambda\tau}]\lambda \\ & + \gamma^2(1 - G + Q + I + aI + aI^2 - aGI \\ & \qquad + QI - (1 + I + aI + aI^2)\kappa e^{-\lambda\tau}). \end{aligned} \tag{7}$$

Note that for $\kappa = 0$ this characteristic equation reduces to the eigenvalue equation of the Yamada system [5].

While the analysis of (7) is generally quite difficult, we can make the following observations.

Proposition 1. *In the (τ, κ)-plane one finds the following two local bifurcations along horizontal lines:*

(i) the locus T of transcritical bifurcations, given by

$$\kappa_T(A, B) = 1 - A + B, \tag{8}$$

where the equilibria E_1 and E_2 meet on the invariant line $\{I = 0\}$. For $\kappa < \kappa_T$ both E_1 and E_2 exist (in the region where $I \geq 0$), and E_1 is attracting. For $\kappa > \kappa_T$ only E_1 exists (in the region where $I \geq 0$), and it is a saddle point.

(ii) the locus S of saddle-node bifurcations, given by

$$\kappa_S(A, B, a) = \frac{-aA + a - B - 1 + 2\sqrt{aAB}}{a - 1}, \tag{9}$$

where the equilibria E_2 and E_3 bifurcate. For $\kappa < \kappa_S$ the system possesses just the equilibrium E_1; for $\kappa > \kappa_S$ also the equilibria E_2 and E_3 exist, of which E_2 is always a saddle point (in the region where $I \geq 0$).

Proof. For statement (i) we consider the equilibrium E_1, where $(G, Q, I) = (A, B, 0)$, so that (7) reduces to

$$\begin{aligned} 0 &= \lambda^3 + \left[1 - A + B + 2\gamma - \kappa e^{-\lambda\tau}\right]\lambda^2 \\ &\quad + \left[\gamma^2 + 2\gamma - 2\gamma A + 2\gamma B - 2\gamma\kappa e^{-\lambda\tau}\right]\lambda \\ &\quad + \gamma^2\left(1 - A + B - \kappa e^{-\lambda\tau}\right). \end{aligned}$$

The condition that $\lambda = 0$ is a root immediately gives (8). The existence of E_2 with $I \geq 0$ for $\kappa < \kappa_T$ follows from (6), and the stability of E_1 was checked numerically with DDE-BIFTOOL by inspecting the change of roots of the characteristic equation across S.

For statement (ii) one needs to consider a root $\lambda = 0$ of the full characteristic equation, that is, a root of the last term of (7). A simpler alternative is to realize that a saddle-node bifurcation corresponds to the square root in (6) being zero, that is,

$$0 = (aA - B - a - 1 + a\kappa + \kappa)^2 - 4a(\kappa - 1)(A - B - 1 + \kappa),$$

and (9) follows. The stability of the bifurcating equilibria E_2 and E_3 was again checked numerically with DDE-BIFTOOL. □

It follows from (8) that the transcritical locus T only lies in the physically relevant part of the (τ, κ)-plane, meaning that $\kappa_T \geq 0$, provided that

$$A \leq B + 1.$$

Note that equality above gives exactly the condition that there is a transcritical bifurcation in the Yamada model; see Ref. [5, Appendix A]. In other words, the transcritical locus T only occurs for $\kappa \geq 0$ provided that A is chosen to lie to the left of the curve T in Figure 2(b). Similarly, (9) implies that the saddle-node locus S is such that $\kappa_S \geq 0$ provided that

$$A \leq \frac{(-1 + a + 2\sqrt{(a-1)B} + B)}{a}.$$

Equality above gives exactly the condition that there is a saddle-node bifurcation in the Yamada model; see Ref. [5, Appendix A]. Hence, the saddle-node locus S only occurs for $\kappa_S \geq 0$ provided that A is chosen from region 1, to the left of the saddle node locus S in Figure 2(b). We remark that $\kappa_S \leq 1$ is always satisfied, which means that (6) does actually not become singular at either E_2 or E_3.

The equilibrium E_3 may lose its stability in a Hopf bifurcation. The ansatz that there is a purely imaginary root $\lambda = i\omega$ of the characteristic equation (7)

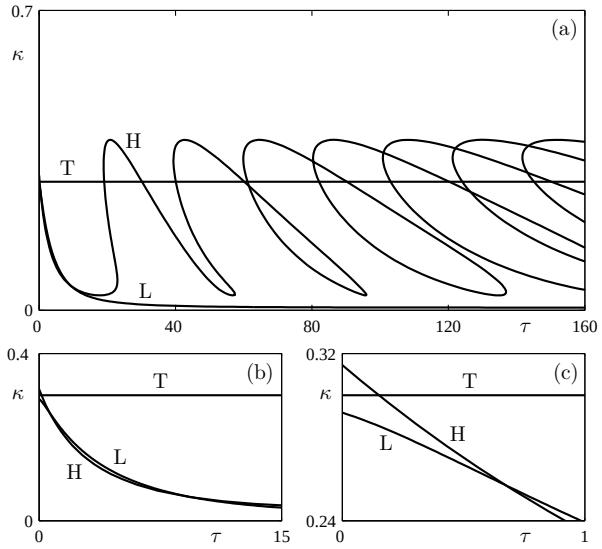

Figure 5: Computed bifurcation diagram in the (τ, κ)-plane for $A = 6.5$ (a); panels (b) and (c) are two successive enlargements. Shown are the transcritical curve T, a Hopf curve H, and a homoclinic loop curve L.

leads to a complicated transcendental equation for the locus of Hopf bifurcation. As the bifurcation diagrams in the next sections will show, there is not a simple formula for this locus, which may consist of infinitely many disjoint curves of Hopf bifurcation in the (τ, κ)-plane. Rather than computing them numerically from (7), we compute the curves of Hopf bifurcation with the continuation package DDE-BIFTOOL; this is equivalent, because DDE-BIFTOOL also solves the characteristic equation numerically, albeit in implicit form [25, 28].

4 Bifurcation study for excitable SLSA

We now study the influence of the feedback loop on phase portrait 2 of the Yamada model, where the off-state of the laser is a global attractor and the system is excitable; see Figure 4. To this end, we fix the gain pump parameter at $A = 6.5$, to the left of the transcritical curve in Figure 2(b). (Recall that $B = 5.8$, $a = 1.8$ and $\gamma = 0.04$ are fixed.) For this value of A the transcritical locus T, but not the saddle-node locus S, can be found in the physically relevant region where $\kappa \geq 0$; see Proposition 1.

Figure 5 shows the computed bifurcation diagram of Eqs. (1)–(3) in the (τ, κ)-plane. Apart from the horizontal curve T at $\kappa_T = 1 - A + B = 0.3$, the figure shows a single, connected Hopf curve H and a homoclinic loop curve L. The curve H has more and more self-intersections for larger values of τ; each such intersection is a Hopf-Hopf bifurcation point where the system possesses

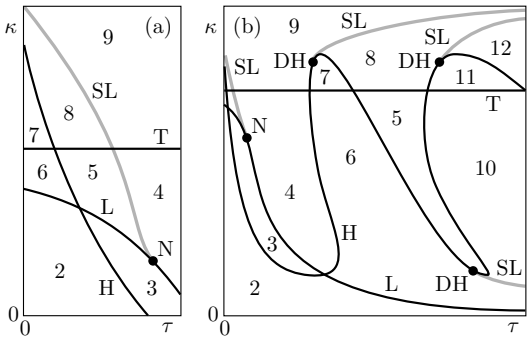

Figure 6: Sketches of the bifurcation diagram in the (τ, κ)-plane for $A = 6.5$; panel (a) is up to small and panel (b) up to an intermediate value of τ. The grey curves SL are loci of saddle-node of limit cycle bifurcations; numbered regions correspond to phase portaits in Figure 3.

two pairs of purely complex conjugate eigenvalues. The homoclinic loop curve L crosses the Hopf curve H twice; see the enlargements in Figure 5(b) and (c). The curve L then appears to approach the line $\kappa = 0$ as $\tau \to \infty$.

Figure 6 shows two qualitative sketches of this bifurcation diagram in the (τ, κ)-plane. Panel (a) is for quite small values of τ up to about 1; compare with Figure 5(c). Figure 6(b) is for intermediate values of τ up to about 60; compare with Figure 5(a). This range of the (τ, κ)-plane is most relevant from the applications point of view, because we are interested in self-pulsations of high frequency (hence, τ should not be too large). The new features in Figure 6 are (grey) curves SL of sadddle-node bifurcation of limit cycles: one emanates from a codimension-two point N on the curve L where the saddle is neutral, and the other curves SL emanate from degenerate Hopf points DH on the Hopf curve H. At each such point the Hopf bifurcation changes criticality, meaning that the bifurcating periodic orbit changes form being attracting to being of saddle type. Because it is quite difficult to follow a sadddle-node bifurcation of limit cycles in a DDE, we verified the positions of the curves SL with careful numerical simulations of Eqs. (1)–(3). We also found that the Hopf bifurcation curve H and the homoclinic loop curve L both change criticality very close to where they cross for lower values of κ; in fact, this happens practically at their intersection point within the accuracy of our investigation, and no additional curve SL could be found.

The sketched bifurcation curves in Figure 6 constitute a conjectured partial bifurcation diagram in the shown part of the (τ, κ)-plane; it is complete enough to allows us to identify the numbered regions with different phase portraits that can be found in Figure 3. Notice that region 2 of excitable dynamics is immediately adjacent to the line $\{\kappa = 0\}$; this is expected for our choice of A because the DDE for $\kappa > 0$ is a regular perturbation of the ODE for $\kappa = 0$. What is more, for small τ we find a bifurcation structure that is very much

like that in the (A, γ)-plane of type III; compare Figure 6(a) with Figure 2(a). In particular, phase portraits 2–9 (that is, all phase portraits of the Yamada system with the exception of that in region 1) can be found in the corresponding regions. In other words, near the limit $\tau = 0$ the delay time τ and the feedback strength κ unfold the dynamics in a similar way as gain pump paramter A and time-scale separation parameter γ when $\tau = \kappa = 0$. Already for intermediate values of τ as in Figure 6(b), on the other hand, we find a bifurcation structure that is more complicated, with additional dynamics in regions 10–12. Note from Figure 3 that these new phase portraits can still be drawn in a two-dimensional plane. All these phase portraits have stable oscillations; their new feature is the existence of additional nested periodic orbits.

For intermediate values of the feedback strength around $\kappa = 0.2$ one finds a characteristic transition as the delay time τ is increased; see Figure 3 for the phase portraits that are encountered. For small τ in regions 2 the laser is excitable. When the curve H is crossed into region 3 as τ is increased, a periodic orbit of saddle type is created around the bifurcating equilibrium, which is now stable. Hence, the laser is bistable: it is still excitable when it is in the off-state with $I = 0$, but for suitable initial conditions it may also emit light at the constant intensity value of the stable equilibrium with $I > 0$. When the curve L is crossed and region 4 is entered, the unstable periodic orbit disappears; the system is still bistable but no longer excitable: any sufficiently large perturbation of the off-state now brings the laser into the basin of attraction of the stable equilibrium with $I > 0$. When τ is increased further, the curve H is crossed a second time. Now a stable periodic orbit is born along H so that in region 6 we now find bistability between the off-state and self-sustained oscillations. As τ is increased even further, the Hopf bifurcation curve H is crossed several more times; this leads to the creation of more periodic orbits, which are alternatingly attracting and of saddle type. As Figure 5(a) clearly shows, the bifurcation diagram becomes increasingly complicated for even larger values of τ — so much so that it becomes impractical to map out all regions of different dynamics.

An important new aspect of the bifurcation diagram in Figure 6(b) is the fact that region 6, where one finds bistability between the off-state and self-pulsations, is now so large that it becomes experimentally accessible. It can be reached, for example, from region 2 by increasing κ for a fixed intermediate value of the delay time τ, or from region 4 by increasing τ for suitable fixed κ. The relevant region in the (τ, κ)-plane is shown enlarged in Figure 7(a). Panel (b) shows the period of the attracting periodic orbit Γ as it is continued in the direction of decreasing κ from the point p on the Hopf curve H. As is to be expected, the period of Γ increases and diverges to infinity as the homoclinic loop curve L is approached. Panels (c1)–(c3) of Figure 7 show the response of the system to a sufficiently large perturbation (above the stable manifold of the saddle point in region 6). After an initial large pulse, the system settles down to the attracting periodic orbit and, hence, produces regular oscillations. As the curve L is approached, these oscillations take the form of self-pulsations with clearly defined pulses. Indeed, the interspike time (which is the period of the periodic orbit) increases as κ is decreased towards the curve L.

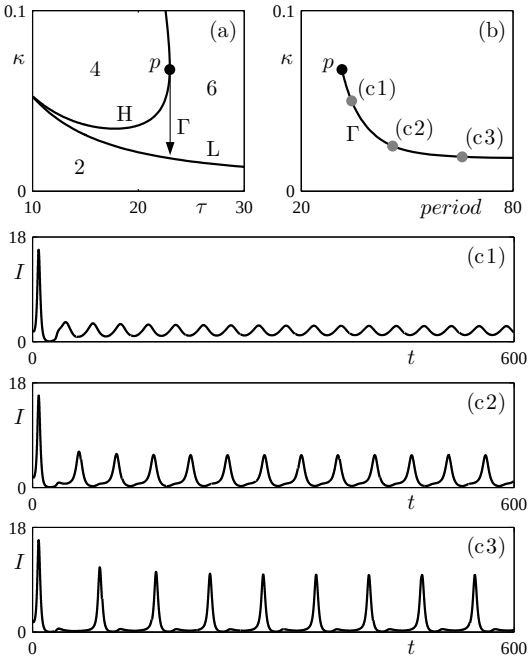

Figure 7: Panel (a) shows a region of the (τ, κ)-plane with transition to region 6. Panel (b) shows the period of the periodic orbit Γ in region 6 as continued from the point p of the Hopf curve H towards the homoclinic loop curve L. Panels (c1), (c2) and (c3) show associated time series after a sufficiently large perturbation from the stable off-state.

5 Bifurcation study for non-excitable SLSA

We now consider the influence of the feedback loop on phase portrait 1 of the Yamada model, where the off-state of the laser is a global attractor but the system is not excitable; see Figure 3. Figure 8(a) shows the relevant computed bifurcation diagram of Eqs. (1)–(3) in the (τ, κ)-plane for $A = 5.9$, a value somewhat to the left of the saddle-node curve S in Figure 2(b). (Again, $B = 5.8$, $a = 1.8$ and $\gamma = 0.04$ are fixed.) Hence, according to Proposition 1 we find the saddle-node locus S as the horizontal line at $\kappa_S \approx 0.09578$. The line S bounds a horizontal strip near $\kappa = 0$ where one finds phase portrait 1 for any τ; again, this is to be expected from the fact that the DDE is a regular perturbation of the Yamada system. In contrast to the case for $A = 6.5$ in Figure 5(a), for $A = 5.9$ the locus of Hopf bifurcation is no longer a single curve. Figure 8(a) actually shows several disjoint Hopf curves that intersect in numerous double Hopf points; along the shown curves H one finds a Hopf bifurcation at the equilibrium E_3. Note further that the transcritical locus T no longer intersects the Hopf curves H; it lies at $\kappa_T = 0.9$, which is outside the range shown in

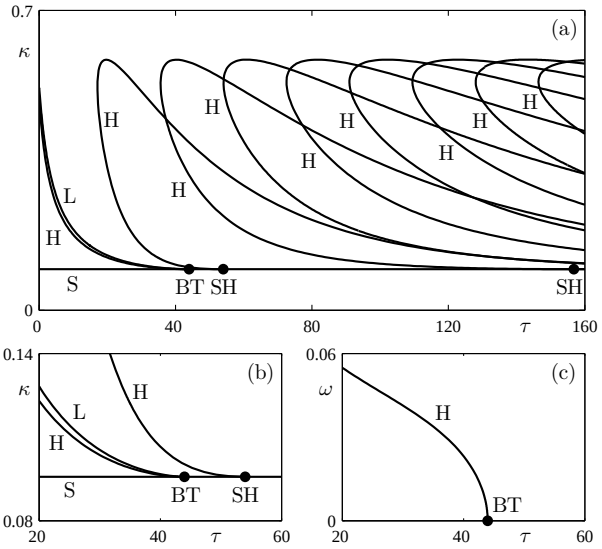

Figure 8: Computed bifurcation diagram in the (τ, κ)-plane for $A = 5.9$ (a), and an enlargement near a Bogdanov-Takens point BT and a saddle-node Hopf point SH (b). Shown are the saddle-node curve S, Hopf curves H, and a homoclinic loop curve L. Panel (c) shows the imaginary part ω along the Hopf curve that ends at the point BT.

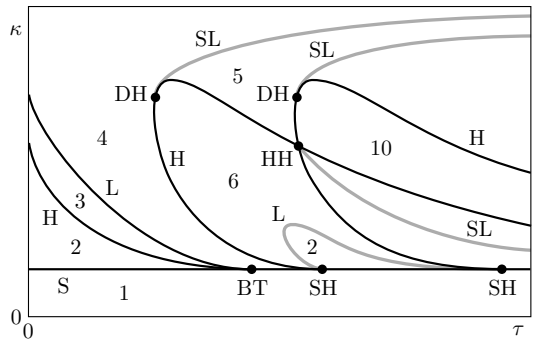

Figure 9: Sketch of the bifurcation diagram in the (τ, κ)-plane for $A = 5.9$. The grey curves SL are loci of saddle-node of limit cycle bifurcations, and the grey curve L is another curve of homoclinic loops; for phase portaits in numbered regions see Figure 3.

Figure 8(a).

Another new feature of Figure 8(a) are codimension-two points on the saddle-node line S. There are a Bodganov-Takens point BT (where the system has a double-zero eigenvalue) and two codimension-two saddle-node Hopf points

SH (where there is a zero eigenvalue and a complex conjugate pair of purely imaginary eigenvalues) [29, 30]. These points are end points of Hopf curves. Panel (c) shows that the imaginary part ω along the Hopf curve H decreases to zero as the point BT is approached, which is evidence for the fact that one is indeed dealing with a Bodganov-Takens point. As was also checked, the imaginary part ω along the respective Hopf curves tends to a nonzero limit at the points SH. Notice also that the homoclinic loop curve L ends at the point BT; see Figure 8(b).

Figure 9 shows a qualitative sketch of the partial bifurcation diagram for $A = 5.9$. As before, we added a number of bifurcation curves that are very difficult to continue directly in the DDE, but must exist near the known codimension-two bifurcation points; existence and positions of these curves was again verified by careful numerical simulations of Eqs. (1)–(3). There are two (grey) curves SL of sadddle-node bifurcation of limit cycles emanating from codimension-two degenerate Hopf points DH, and one (grey) curve SL emanating from a codimension-two Hopf-Hopf point HH. Furthermore, we also added an additional homoclinic loop curve L that connects the two points SH and bounds a second region where one finds the excitable phase portrait 2.

Figure 9 is meant to show what additional bifurcation curves are involved in the interaction of the three left-most Hopf curves of the bifurcation diagram in Figure 8(a). Indeed, many more additional Hopf curves and codimension-two points HH exist, meaning that the sketch in Figure 9 does not give a complete division of the (τ, κ)-plane into regions of different dynamics. Nevertheless, it is complete enough to allow us to identify the regions where one finds portraits 1–6 and 10 from Figure 3.

6 Dependence of the bifurcation diagram on the gain pump parameter

The two bifurcation diagrams in the (τ, κ)-plane for $A = 5.9$ and $A = 6.5$, in Figure 8(a) and Figure 5(a), respectively, are clearly qualitatively different. Yet, since they depend only on the gain pump parameter A, changing A from $A = 5.9$ to $A = 6.5$ (or vice versa) transforms the two bifurcation diagrams into one another. We now describe briefly how this happens via the transition through codimension-three bifurcations. Here we take a geometric approach that is supported by numerical computation with DDE-BIFTOOL.

The overall features of this transition when A is increased through the interval $A \in [5.9, 6.5]$ can be described as follows.

- the different Hopf curves for $A = 5.9$ merge into the single Hopf curve for $A = 6.5$;
- the codimension-two points BT and SH disappear towards infinite values of τ;
- the curve S disappears when A reaches the curve S in Figure 2(b) at $A = (-1 + a + 2\sqrt{(a-1)B} + B))/a$; and

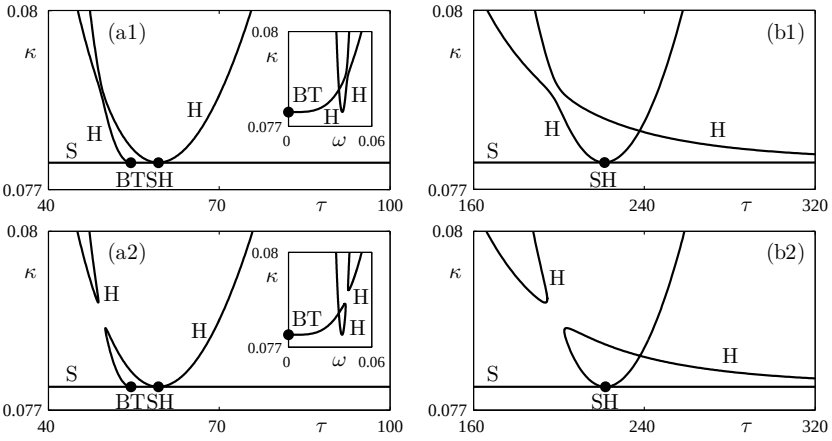

Figure 10: Before (top) and after (bottom) a saddle-transition of Hopf curves H, near BT and SH (a) and near SH (b); insets in panels (a1) and (a2) show the imaginary part ω at the Hopf curves H. These bifurcation diagrams have been computed with DDE-BIFTOOL, where A has the values 5.9311 in (a1), 5.9312 in (a2), 5.9311 in (b1), and 5.9312 in (b2).

- the transcritical curve T moves down and starts to intersect the curve H.

We concentrate here on the bifurcations of the Hopf curves as the main ingredients in the transition for $A \in [5.9, 6.5]$. To this end, we now consider all Hopf curves for $A = 5.9$ — including those where the bifurcation takes place at E_2, which are not shown in Figures 8(a) and 9.

As A is increased, one finds values of A where the connectivity between different branches of Hopf curves in the (τ, κ)-plane changes locally; we speak of a saddle transition of Hopf curves. Figure 10 shows two examples of this bifurcation, which is of codimension three. More specifically, Figure 10(a1) and (a2) show the bifurcation diagram before and after a saddle transition of Hopf curves near the points BT and SH; the inset panels show the purely imaginary parts of the bifurcating eigenvalues along the Hopf curves. Notice how two separate Hopf bifurcation curves that end at BT and SH, respectively, connect differently, creating a direct connection from BT to SH. Figure 10(b1) and (b2) show a saddle transition of Hopf curves near the point SH for larger values of τ. The result is again a different connectivity of Hopf curves H near the point SH. A saddle-transition of Hopf curves is a bifurcation of codimension three because it changes the topological type of the bifurcation diagram in the (τ, κ)-plane at a single discrete value of A. This bifurcation has been found in transitions between different two-parameter bifurcation diagrams in other laser systems; see, for example, [32, 33]. When seen in (τ, κ, A)-space, a saddle-transition of Hopf curves corresponds to the transition of a plane given by $A = const$ through a saddle-point of the two-dimensional surface $H(\tau, \kappa)$ of Hopf bifurcation; here a saddle point is given by the condition that $\operatorname{grad} H = 0$ and the determinant

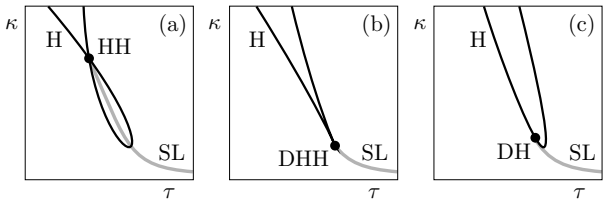

Figure 11: Sketch of the transition through a codimension-three degenerate Hopf-Hopf point DHH, where a loop in a Hopf curve H with a point HH tansforms into a lobe with a point DH.

of the Hessian is negative.

After the saddle transitions of Hopf curves in Figure 10, the codimension-two points BT and SH are 'free to move' towards larger values of τ as A is increased further. In the process they 'drag' the other bifurcation curves with them towards larger values of τ. In this way, the homoclinic loop curve L ending at BT (not shown in Figure 10) becomes the lower boundary of the bifurcation diagram; compare with Figure 5(a). With increasing A the saddle-node curve S moves down in κ and finally disappears at $A = (-1 + a + 2\sqrt{(a-1)B} + B))/a$ into the (unphysical) region of negative κ.

Relating the saddle transition in Figure 10(b1) and (b2) back to the larger picture in Figure 9 shows that this transition results in a Hopf curve H with a loop, where the self-intersection point is the sketched Hopf-Hopf point. Investigation with DDE-BIFTOOL shows that, when A is increased beyond the value 5.9312, then this loop changes into the 'lobe' with a point DH that one finds in Figure 6(b). The mechanism is the transition through a codimension-three degenerate Hopf-Hopf bifurcation point DHH, and it is sketched in Figure 11. At the moment of bifurcation in panel (b), the Hopf curve has a cusp, which is the point DHH.

7 Conclusions

We presented a bifurcation study of the influence of an optical feedback loop on a semiconductor laser with a saturable absorber as modeled by the Yamada ODE. The resulting DDE model was studied by means of linear stability analysis of its equilibria in combination with a bifurcation analysis with the continuation package DDE-BIFTOOL. More specifically, bifurcation diagrams in the plane of delay time τ and feedback strength κ were presented for two relevant choices of the gain pump parameter A. The transition of the bifurcation diagram in the (τ, κ)-plane with A was discussed in terms of transitions through certain codimension-three bifurcations.

The work presented here can be seen as a case study of how a laser system with delay can be investigated with tools from bifurcation theory and, in particular, with numerical continuation as implemented, for example, in the package

DDE-BIFTOOL. The physical motivation for this work is the wish to use the additional control parameters τ and κ to ensure reliable self-pulsations of the overall system with small timing jitter. To this end, the bifurcation diagram in the (τ, κ)-plane was considered for a small range of the gain pump parameter A near the region where the SLSA without delay is excitable. In this way, we identified large and experimentally accessible additional regions where the SLSA produces a stable train of pulses in the presence of the optical feedback loop.

Indeed, this study is far from complete and there are several directions for future research. First of all, an investigation of the influence of noise on dynamics of the SLSA with delay would be the logical next step to determine the timing properties of the corresponding pulse trains under more realistic conditions. Secondly, we restricted our attention to a relatively small range of the delay time τ. As a result, the phase portraits we found for the SLSA with delay are all quite special in that they can be drawn by planar phase portraits, where the missing (infinitely-many) directions are strongly attracting. A more wide-ranging bifurcation analysis, in dependence of A as well as on other parameters of the Yamada system, would be expected to result in the discovery of more complicated dynamics.

References

[1] Krauskopf B. and Lenstra D. (Eds.) [2000] *Fundamental Issues of Nonlinear Laser Dynamics*, AIP Conf. Proc. Vol. 548 (American Institute of Physics Publishing, Melville, NY).

[2] Kane D. M. and Shore K. A. (Eds.) [2005] *Unlocking Dynamical Diversity: Optical Feedback Effects on Semiconductor Lasers* (Wiley).

[3] Antoranz J. C., Gea, J. and Velarde M. G. [1981] "Oscillatory phenomena and Q-switching in a model for a laser with a saturable absorber," *Phys Rev Lett* **47**, 1895–1898.

[4] T. Erneux [1988] "Q-switching bifurcation in a laser with a saturable absorber", *JOSA B* **5**, 1063–1069.

[5] Dubbeldam J. L. A. and Krauskopf B. [1999] "Self-pulsations of lasers with saturable absorber: dynamics and bifircations," *Opt Commun* **159**, 325–338.

[6] Mandel P. [1997] *Theoretical Problems in Cavity Nonlinear Optics*, Cambridge Studies in Modern Optics, (Cambridge University Press).

[7] Kawaguchi H. [1994] *Bistabilities and Nonlinearities in Laser Diodes*, (Artech House).

[8] Georgiou M. and Erneux T. [1992] "Self-pulsating laser oscillations depend on extremely small amplitude noise," *Phys Rev A* **45**, 6636–6642 .

[9] Dubbeldam J. L. A., Krauskopf B. and Lenstra D. [1999] "Excitability and coherence resonance in lasers with saturable absorber," *Phys Rev E* **60**, 6580–6588.

[10] Murray J.D. [1990] *Mathematical Biology*, (Springer-Verlag, New York).

[11] Grill S., Zykov V.S. and Müller S.C. [1996] "Spiral wave dynamics under pulsatory modulation of excitability," *J Phys Chem* **100**, 19082–19088.

[12] Taylor D., Holmes P. and Cohen A.H. [1997] "Excitable oscillators as models for central pattern generators," *Series on stability, Vibration and Control of Systems, Series B*, (World Scientific Publishing Company, Singapore).

[13] Tredicce J. R. [2000] "Excitability in laser systems: the experimental side," in [1], pp. 238–259.

[14] Wieczorek S. M., Krauskopf B. and Lenstra D. [2002] "Multipulse excitability in a semiconductor laser with optical injection," *Phys Rev Lett* **88**, 063901.

[15] Mullet J. and Mirasso C. R. [1999] "Numerical statistics of power dropouts based on the Lang-Kobayashi model," *Phys Rev E* **59**, 5400–5405.

[16] Yacomotti A. M., Eguia M. C., Aliaga J., Martinez O. E., Mindlin G. B. and Lipsich A. [1999] "Interspike time distribution in noise driven excitable systems," *Phys Rev Lett* **83**, 292–295.

[17] Wünsche H.-J., Brox O., Radziunas M. and Henneberger F. [2002] "Excitability of a semiconductor laser by a two-mode homoclinic bifurcation," *Phys Rev Lett* **88**, 023901.

[18] Tronciu V. Z., Wünsche H.-J., Radziunas M. and Schneider K. R. [2001] "Excitability of lasers with integrated dispersive reflectors," *Proceedings of SPIE* **4283**:347.

[19] Krauskopf B., Schneider K. R., Sieber J., Wieczorek S. M. and Wolfrum M. [2003] "Excitability and self-pulsations near homoclinic bifurcations in semiconductor laser systems," *Opt Commun* **215**, 367–379.

[20] Yamada M. [1993] "A theoretical analysis of self-sustained pulsation phenomena in narrow stripe semiconductor lasers," *IEEE J Quantum Electron* **QE-29**, 1330–1336.

[21] Jones C. K. R. T. [1995] *Geometric Singular Perturbation Theory. Dynamical Systems (Montecatini Terme, 1994)*, Springer Lecture Notes in Mathematics **1609**, (Springer-Verlag, New-York), pp. 44–118.

[22] Hale J. K. & Verduyn Lunel S. M. [1993] *Introduction to Functional Differential Equations* (Springer-Verlag, New York).

[23] Diekmann O., Van Gils S. A., Verduyn Lunel S. M. and Walther H. O. [1995]
Delay Equations: Functional-, Complex- and Nonlinear Analysis, (Springer-Verlag, New York).

[24] Verduyn Lunel S.M. and Krauskopf B. [2000] "The mathematics of delay equations with an application to the Lang-Kobayashi equations," in [1], pp. 66–87.

[25] Engelborghs K., Luzyanina T., Samaey G. and Roose D. [2001] "DDE-BIFTOOL: a Matlab package for bifurcation analysis of delay differential equations," Tech. Rep. TW-330 Department of Computer Science, K. U. Leuven, Belguim; available from `http://www.cs.kuleuven.ac.be/cwis/research/twr/research/software/delay/ddebiftool.shtml`

[26] Szalai R. [2005] *PDDE-CONT: A continuation and bifurcation software for delay-differential equations,* Budapest University of Technology and Economics, Hungary; available from `http://www.mm.bme.hu/~szalai/pdde`

[27] Krauskopf B. [2005] "Bifurcation analysis of lasers with delay," in [2], pp. 147-183.

[28] Roose D. and Szalai R. [2007] "Continuation and bifurcation analysis of delay differential eqautions," in Krauskopf B., Osinga H. M. and Galán-Vioque J. (Eds.) *Numerical Continuation Methods for Dynamical Systems: Path following and boundary value problems*, (Springer-Verlag, New York), pp. 359–399.

[29] Guckenheimer J. and Holmes P. [1986] *Nonlinear Oscillations, Dynamical Systems and Bifurcations of Vector Fields*, Second Printing, (Springer-Verlag, New York).

[30] Kuznetsov Yu. A. [1992] *Elements of Applied Bifurcation Theory*, (Springer-Verlag, New York).

[31] Doedel E. J. and Oldeman B. E. with major contributions from Champneys A. R., Dercole F., Fairgrieve T. F., Kuznetsov Yu. A., Paffenroth R. C., Sandstede B., Wang X. J. and Zhang C. H. [2010] *AUTO-07p Version 0.7: Continuation and bifurcation software for ordinary differential equations*, (Department of Computer Science, Concordia University, Montreal, Canada); available from `http://cmvl.cs.concordia.ca/auto/`

[32] Green K. and Krauskopf B. [2004] "Bifurcation analysis of a semiconductor laser subject to non-instantaneous phase-conjugate feedback," *Optics Communications* **231**, 383–393.

[33] Erzgräber, Krauskopf B. and Lenstra D. [2007] "Bifurcation analysis of a semiconductor laser with filtered optical feedback," *SIAM J Appl Dynam Syst* **6**, 1–28.